Formation mechanism of a microscale domain and effect on transport properties in strained VO$_2$ thin films on TiO$_2$(001)

Kenichi Kawatani, Teruo Kanki,[*] and Hidekazu Tanaka[*]

Institute of Scientific and Industrial Research, Osaka University, 8-1 Mihogaoka, Ibaraki, Osaka 567-0047, Japan
(Received 17 June 2014; revised manuscript received 24 July 2014; published 11 August 2014)

We investigated film thickness dependence of domain size and transport property in VO$_2$ thin films on rutile TiO$_2$ (001) substrates and identified formation mechanism of the microscaled domain. It was found that domain size decreased with increasing film thickness and the domain boundary consisted of cracks and dislocations, clarified by high-resolution transmission electron microscopy. The detailed images showed, the tensile-strained VO$_2$ lattices received by TiO$_2$ (001) were partially relaxed around the cracks and dislocations. The relaxed lattice is likely to return the original metal-insulator transition temperature of 340 K, whereas the tensile-strained lattice has the transition at 300 K in a VO$_2$/TiO$_2$ (001) system. Thus, the mixed states of strained and relaxed crystal lattice and the increase in dislocation density in thicker films cause the overly broad resistance behavior against temperature. Furthermore, the origin of the dislocations and the thickness dependence of the domain size could be explained by the energy release of shear stress generated by competition between the pinning layers at near-interface VO$_2$ layers holding the tetragonal structure and the near-surface layers separated from the substrate attempting the lattice transformation to a monoclinic structure. This understanding enables us to more precisely design the size and configuration of these domains and their transport properties.

PACS number(s): 74.62.−c, 68.35.Rh, 68.03.Cd

I. INTRODUCTION

Vanadium dioxide (VO$_2$) has attracted much attention because of its metal-insulator transition (MIT) with orders of magnitude change in resistance at 340 K accompanied by structural deformation between an insulating monoclinic phase at lower temperature and a metallic tetragonal rutile phase at higher temperature. In this system, the metallic and insulating domains often coexist randomly around the transition temperature, and each domain works as an essential element invoking first order MIT [1–3] and influences the macroscopic transport property. The domain size ranges from several tens of nanometers [4–6] to the micrometer scale [7–11]. Recent reports have revealed that, in oxide materials with mixed domains, the elastic strain caused by lattice distortion or mismatch between the substrate and thin film can greatly impact their domain characteristics and electronic properties [7,12–15]. Other reports have shown that bending VO$_2$ beams can generate microscale domains shaped like triangular and rectangular patterns [16–18] and that stress can modulate the metal-insulator transition temperature (T_{MI}) [16]. In VO$_2$ thin films on rutile TiO$_2$ (001) substrates, strain caused by lattice mismatch between the film and substrate can shift T_{MI} from 340 K to ∼300 K [13,14]. Recently, in the VO$_2$/TiO$_2$ (001) system we have observed the presence of giant microscale metallic domains with rectangular shapes and the first order transition induced within individual domains [2,9–11]. Optical microscopy has been used to identify how the transport properties are changed by the MIT of each domain, supporting the relationship between the domain configurations and their electronic properties [2,9–11]. Moreover, we showed that changing the size and aspect ratio of VO$_2$ thin films on TiO$_2$ (001) in relation to the domain configuration can

significantly modulate transport properties [11]. On the other hand, it remains poorly understood how microscale domains form in VO$_2$ thin films on rutile TiO$_2$ (001) substrates. Clarifying the origin of these domains would enable us to better control the domain shape and size, and their transport properties. In this research, we investigated the domain size depending on the film thickness and identified the formation mechanism of the domain structure by assessing the shear stress generated by competition between the pinning layers at near-interface VO$_2$ layers holding the tetragonal structure and the near-surface layers separated from the substrate attempting the lattice transformation to a monoclinic structure.

II. EXPERIMENT

VO$_2$ thin films were deposited on rutile TiO$_2$ (001) substrates using pulsed laser deposition (ArF excimer laser, $\lambda = 193$ nm) at 430 °C and 1.0 Pa oxygen pressure at a laser repetition rate of 2 Hz with energy fluency of 10 mJ/cm^2. A V$_2$O$_5$ pellet was used as the target. The deposition rate was approximately 0.3 nm/min. VO$_2$ grown on TiO$_2$ (001) substrate has a tetragonal (001) plane, represented by two significant peaks of tetragonal VO$_2$ (002) at a higher angle and TiO$_2$ (002) at a lower angle, as in the inset of Fig. 1. The thickness of these films ranged from 10 to 50 nm, measured by atomic force microscopy. Figure 1 shows the temperature dependence of normalized resistance in various thick VO$_2$ thin films on TiO$_2$ (001) substrates. The 10-nm-thick film indicates abrupt MIT around 295 K in the heating process. With increasing film thickness, MIT shows steplike behavior in the 15- and 25-nm-thick films then broadens in the 50-nm-thick film, and the transition temperature increases. This tendency is almost the same as reported in Ref. [14].

An optical microscope (VH-Z500R, Keyence) equipped with a Peltier-based temperature-controlled stage (T95, Linkam) was used to distinguish the metallic and insulating

---

*Corresponding authors: kanki@sanken.osaka-u.ac.jp; h-tanaka@sanken.osaka-u.ac.jp
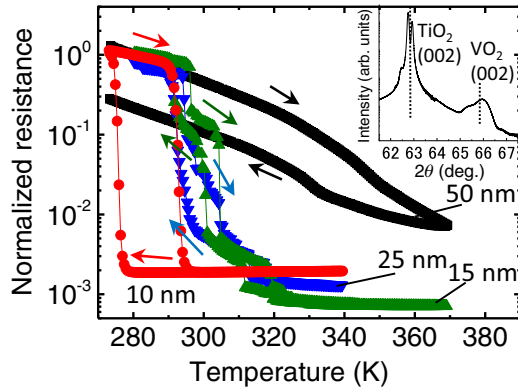
FIG. 1. (Color online) Temperature dependence of normalized resistance in 10- (red circles), 15- (green triangles), 25- (blue inverse triangles), and 50-nm-thick (black squares) VO$_2$ thin films on TiO$_2$ (001) substrates. Inset shows an x-ray diffraction pattern of a 15-nm-thick VO$_2$ thin film on a TiO$_2$ (001) substrate.

domains at a submicrometer resolution by comparing the reflectance of those domains at optical wavelengths [19]. High-resolution transmission electron microscopy (HRTEM; H-9000NAR, Hitachi High-Technologies Corporation) was performed by the Foundation for Promotion of Material and Science and Technology (MST) of Japan.

III. RESULTS AND DISCUSSION

Figure 2 shows optical micrographs of the VO$_2$ thin films at 300 K. Metallic domains shown in a dark color can be easily identified through the evolution when increasing temperature [3]. Film thickness affected the domain size, from several tens of square micrometers in 15-nm-thick films [Fig. 2(b)] to less than 1 μm^2 in the 50-nm-thick films [Fig. 2(d)]. In the 10-nm-thick films [Fig. 2(a)] we found no coexisting domain states within a 50 μm × 50 μm area when temperature crosses the MIT. The color of the domain monolithically and abruptly changes at the MIT, inducing an abrupt change of resistance, as shown in Fig. 1. Most of the domains formed in-plane rectangles along the [110] and [1$\bar{1}$0] directions. The domain size, shape, and position were unchanged in
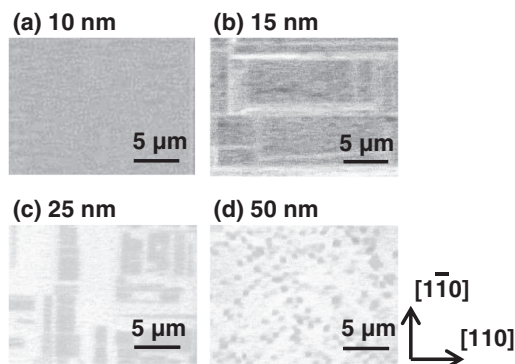
FIG. 2. Optical micrographs of VO$_2$ films on TiO$_2$ (001) substrates at 300 K with thicknesses of (a) 10 nm, (b) 15 nm, (c) 25 nm, and (d) 50 nm in the heating process. The metallic domains shown in these images are darker than the insulating domains.
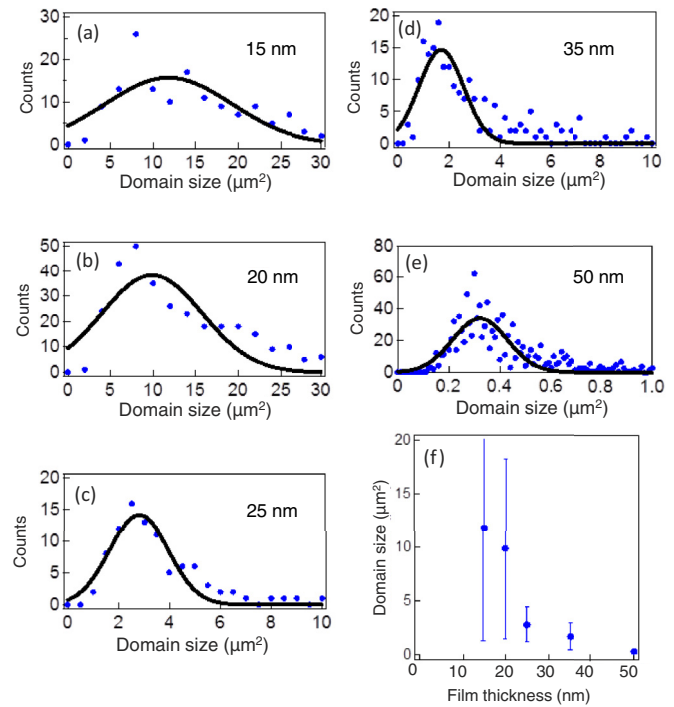
FIG. 3. (Color online) Histograms of domain sizes in VO$_2$ films evaluated from optical micrographs, with thicknesses of (a) 15 nm, (b) 20 nm, (c) 25 nm, (d) 35 nm, and (e) 50 nm. The distributions were fit to Gaussian functions, indicated by bold lines. (f) Dependence of domain size on film thickness, evaluated from the peaks of the Gaussian curves in panels (a)–(e), with error bars indicating the respective standard deviations.

repetitive temperature variation in the thin films on TiO$_2$ (001) substrates [2,6,9]. Thus, we can precisely investigate domain size independently against temperature in various thick VO$_2$ thin films. Figures 3(a)–3(e) show histograms of domain sizes measured from the optical micrographs. Clear peaks exist in these distributions; thus, to find trends in domain size based on film thickness, we fit these distributions to Gaussian functions. Figure 3(f) shows these Gaussian domain size distributions as a function of film thickness. The peak domain size decreased as film size increased, from 11.8 μm^2 in 15-nm-thick films to 0.33 μm^2 in 50-nm-thick films. The full width at half maximum (FWHM) also decreased as film thickness increased.

Cross-sectional HRTEM was used to find the formation mechanism of the domain structure, as shown in Fig. 4(a). This examination revealed cracks near the VO$_2$ surface, as well as dislocations just below the cracks at the boundary, as shown in Fig. 4(b). Regarding sample preparation for the TEM, we first identified the location of domain boundaries with an optical microscope and selected a cutting-plane line for cross-sectional TEM. Location and the number of dislocations and cracks in the wide image of the cross-sectional TEM in the prepared sample approximately correspond to those in the cutting-plane area selected by the optical microscope image. Thus, we conclude that the domain boundary consists of dislocations and cracks as shown in Fig. 4. Dislocations are often produced upon the release of stress, which can be generated by a misfit between lattice constants of the
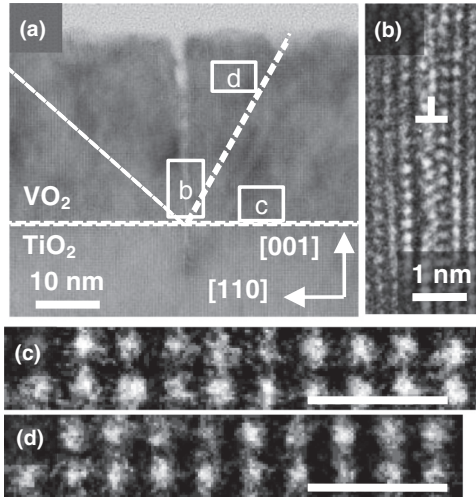
FIG. 4. (a) HRTEM image of a VO$_2$ thin film on TiO$_2$ (001), showing a crack and a dislocation. (b), (c), and (d) Magnified images from points b, c, and d from Fig. 4(a), respectively. The scale bars in (c) and (d) are 1.0 nm.

film and substrate as well as differences between their thermal expansion coefficients [20–22]. Figures 4(c) and 4(d) show evidence of this strain relaxation near the cracks and dislocations in the VO$_2$ thin film on TiO$_2$ (001). The average lattice spacing of VO$_2$ near the interface at point c in Fig. 4(a) is ~0.323 nm, estimated from Fig. 4(c), which is nearly equal to the lattice spacing of the TiO$_2$ substrate estimated from the HRTEM image in Fig. 4(a). In contrast, the lattice spacing of VO$_2$ near the cracks at point d is ~0.313 nm, estimated from Fig. 4(d), which approaches the original lattice spacing of the tetragonal and/or monoclinic VO$_2$ (110). As shown by dashed lines in Fig. 4(a), the relaxation area became wider with distance from the interface, forming an inverse triangle. The transition temperature in the relaxed lattice is likely to return to the original transition temperature of 340 K. Thus, the mixed states of strained and relaxed crystal lattice and the increase of dislocation density in thicker films give the overly broad resistance curve shown in Fig. 1.

It is known that the dislocation density is strongly affected by film thickness. In the typical case, as reported in InGaAs/InP [20,21] and PrBa$_2$Cu3O$_{7-x}$/SrTiO$_3$ [22], the dislocation density decreases with increase film thickness. This trend is opposite in the VO$_2$ thin films on TiO$_2$ (001) as shown in Fig. 3(f); that is, density increases with increasing film thickness. The relationship between dislocation density and film thickness should be distinctive in VO$_2$ on TiO$_2$ (001). The VO$_2$ layers at the interface contained tensile strain in plane with the TiO$_2$ substrate and maintained a rutile structure down to ~300 K [13,14]. This observation is interesting because the T_{MI} of bulk VO$_2$ is 340 K; thus, at 340 K the VO$_2$ layers far from the TiO$_2$ (001) interface should begin transforming into monoclinic insulating states. The main mechanism for dislocation generation would be competition between the pinning layers in near-interface VO$_2$ layers holding the tetragonal structure down to 300 K and the near-surface layers separated from the substrate attempting the lattice transformation to a monoclinic layer at 340 K. During

TABLE I. Lattice spacings along the in-plane (x and y axes) and out-of-plane directions in rutile TiO$_2$ and VO$_2$, as well as in monoclinic VO$_2$.

Crystal structures	x axis (nm)	y axis (nm)	z axis (nm)
Rutile TiO$_2$	$a_{TiO} = 0.4593$	$b_{TiO} = 0.4593$	$c_{TiO} = 0.2959$
Rutile VO$_2$	$a_t = 0.4554$	$b_t = 0.4554$	$c_t = 0.2856$
Monoclinic VO$_2$	$c_m \sin\beta = 0.4535$	$b_m = 0.4526$	$a_m/2 = 0.2877$

the phase transition from tetragonal to monoclinic accompanied by the MIT, the tetragonal phase would hold compressive stress along the in-plane direction, considering the transformation relationship [23,24] and the lattice lengths along the in-plane direction between tetragonal ($a_t = b_t = 4.554$ Å, $c_t = 2.856$ Å) and monoclinic structures ($a_m = 5.753$ Å, $b_m = 4.526$ Å, $c_m = 5.383$ Å, $\beta = 122.6°$) in bulk VO$_2$, as shown in Table I. Now we considered the shear stress of a unit cell (τ_n) in the nth layer generated from the pinning layer, which can be expressed as a function of film thickness ($h = c_t n$),

$$\tau_n = \mu\gamma_n = \frac{0.336}{h}, \qquad (1)$$

where μ is the shear modulus and γ_n is the in-plane-averaged shear strain in the nth layer. The μ value is represented by the equation $\mu = E/2(1 + \nu)$ for isotropic material, where E is Young's modulus, ~140 GPa in VO$_2$ [25], and ν is Poisson's ratio, taken to be 0.3, which is a typical value in solids [14]. Thus, μ is approximately 53.8 GPa, and γ_n is expressed as $\gamma_n = \frac{a_{TiO} - \overline{a_m}}{h} = \frac{0.00625}{h}$, where $\overline{a_m}$ is the averaged in-plane lattice length of monoclinic VO$_2$, that is, $\overline{a_m} = \frac{c_m\sin\beta + b_m}{2}$, estimated from the parameters in Table I. These quantitative values give Eq. (1).

Here the strain energy stored in a unit cell (u_h) can be derived as

$$u_n = \frac{1}{2}\tau_n dx dy \cdot \gamma_n dz = \frac{1}{2}\tau_n\gamma_n V_0 = \frac{6.22 \times 10^{-5}}{h^2} \qquad (2)$$

as a function of h, where V_0 is the volume of a unit cell assuming tetragonal VO$_2$. Thus, the total strain energy (U_t) in a certain volume (V) of an area (S) and a height (h) is given as

$$U_t = \int u_n dS dh = \frac{S}{a_{TiO}b_{TiO}} \int_{h_c}^{h} u_0 dh$$
$$= 2.95 \times 10^{-4} S \left(\frac{1}{h_C} - \frac{1}{h}\right) \qquad (3)$$

by substituting Eq. (2) and the lattice parameters from Table I into Eq. (3).

Here we consider how dislocations are generated. When U_t increases over a critical threshold energy (U_C), which is a characteristic constant value for each material, strain energy should be released by the generation of dislocations. Dislocations mainly form below 340 K during the film fabrication process when cooling the substrate from 700 K to room temperature. In thick films, U_t should be above U_C, causing the lattice to generate dislocations to release the high U_t. Eventually, after generation of dislocations, the relationship between U_t and U_C would be $U_t \leqslant U_C$.
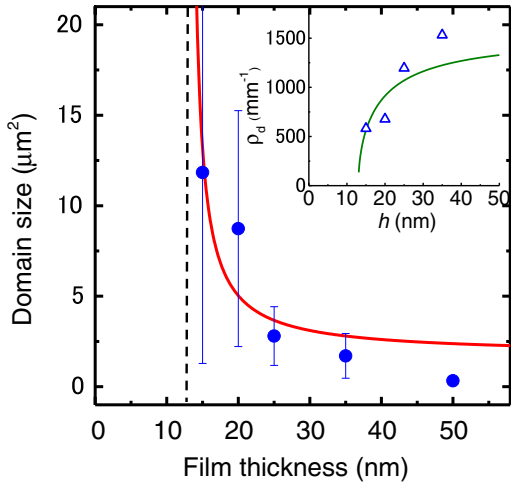
FIG. 5. (Color online) Comparison of domain size calculated from Eq. (4), indicated by the red solid line, with experimental data from Fig. 3(f) when $U_C = 42$. The dashed line indicates h_C (=13 nm). The inset shows film thickness dependence of ρ_d estimated from Eq. (5) in the experimental data (triangle dots) and in Eq. (4) (solid curve).

Finally, we can derive the relationship between S and h using Eq. (3) and the relationship of $U_t \leqslant U_C$ as follows:

$$S \leqslant 3390 U_C \left(\frac{1}{h_C} - \frac{1}{h} \right)^{-1}. \qquad (4)$$

Then, h_C is the critical thickness at which to start generating dislocations, giving 13 nm from our experimental results. Assuming that S is the averaged domain size compartmentalized by dislocations in the VO$_2$ film and appropriately fitting a U_C value to the experimental result in Fig. 3(f), the calculated S from Eq. (4) reflects the experimental trend of film thickness dependence of domain size, as shown in Fig. 5. In addition, the dislocation density (ρ_d), defined as the total length of edge dislocations per unit square, can be approximately estimated

from the relational equation between ρ_d and S:

$$\rho_d = \sqrt{S} \times \frac{1}{S} \left(= \frac{2}{\sqrt{s}} \right). \qquad (5)$$

The $2\sqrt{S}$ and $1/S$ on the right side indicate half the girth of S and the number of domains per unit square, respectively. The inset of Fig. 5 shows ρ_d estimated from Eq. (5) in the experimental data (the triangle dots) and in Eq. (4) (the solid curve) as a function of film thickness. Thus, the untypical relationship between dislocation density and film thickness in the VO$_2$/TiO$_2$ (001) system can be significantly explained by our scenario considering competition between the pinning layers at near-interface VO$_2$ layers and the lattice transformation of near-surface layers separated from the substrate.

IV. CONCLUSION

In summary, we investigated thickness dependence of domain size in detail and the formation mechanism of the domain structure in VO$_2$ thin films on TiO$_2$ (001) substrates. We found that domain size decreased with increasing film thickness and that the domain boundary contained cracks and dislocations. The dislocation density increased with increasing film thickness, as the domain size decreased, showing a different tendency from that in other systems [20–22]. These dislocations formed from the release of strain energy caused by a phase transformation from tetragonal to monoclinic against the pinning tetragonal layer near the interface. Our analysis could reasonably explain how domain size depends on film thickness. This finding allows for more precise modulation of the phase transition temperature, as well as the size and configuration of domains in VO$_2$ films and, thus, their electronic properties.

[1] A. Sharoni, J. G. Ramirez, and I. K. Schuller, Phys. Rev. Lett. **101**, 026404 (2008).

[2] K. Kawatani, H. Takami, T. Kanki, and H. Tanaka, Appl. Phys. Lett. **100**, 173112 (2012).

[3] B. S. Mun, K. Chen, J. Yoon, C. Dejoie, N. Tamura, M. Kunz, Z. Liu, M. E. Grass, S.-K. Mo, C. Park, Y. Y. Lee, and H. Ju, Phys. Rev. B **84**, 113109 (2011).

[4] M. M. Qazilbash, M. Brehm, B. G. Chae, P. C. Ho, G. O. Andreev, B. J. Kim, S. J. Yun, A. V. Balatsky, M. B. Maple, F. Keilmann, H. T. Kim, and D. N. Basov, Science **318**, 1750 (2007).

[5] A. Frenzel, M. M. Qazilbash, M. Brehm, B.-G. Chae, B.-J. Kim, H.-T. Kim, A. V. Balatsky, F. Keilmann, and D. N. Basov, Phys. Rev. B **80**, 115115 (2009).

[6] H. Takami, T. Kanki, and H. Tanaka, Appl. Phys. Lett. **104**, 023104 (2014).

[7] J. Wu, Q. Gu, B. S. Guiton, N. P. de Leon, L. Ouyang, and H. Park, Nano Lett. **6**, 2313 (2006).

[8] A. Tselev, E. Strelcov, I. A. Luk'yanchuk, J. D. Budai, J. Z. Tischler, I. N. Ivanov, K. Jones, R. Proksch, S. V. Kalinin, and A. Kolmakov, Nano Lett. **10**, 2003 (2010).

[9] H. Takami, K. Kawatani, H. Ueda, K. Fujiwara, T. Kanki, and H. Tanaka, Appl. Phys. Lett. **101**, 263111 (2012).

[10] T. Kanki, K. Kawatani, H. Takami, and H. Tanaka, Appl. Phys. Lett. **101**, 243118 (2012).

[11] H. Ueda, T. Kanki, and H. Tanaka, Appl. Phys. Lett. **102**, 153106 (2013).

[12] A. C. Jones, S. Berweger, J. Wei, D. Cobden, and M. B. Raschke, Nano Lett. **10**, 2574 (2010).

[13] Y. Muraoka and Z. Hiroi, Appl. Phys. Lett. **80**, 583 (2002).

[14] K. Nagashima, T. Yanagida, H. Tanaka, and T. Kawai, Phys. Rev. B **74**, 172106 (2006).

[15] Y. Cui and S. Ramanasan, J. Vac. Sci. Technol. A **29**, 041502 (2011).

[16] J. Cao, E. Ertekin, V. Srinivasan, W. Fan, S. Huang, H. Zheng, J. W. L. Yim, D. R. Khanal, D. F. Ogletree, J. C. Grossmanan, and J. Wu, Nat. Nanotechnol. **4**, 732 (2009).

[17] H. Guo, K. Chen, Y. Oh, K. Wang, C. Dejoie, S. A. S. Asif, O. L. Warren, Z. W. Shan, J. Wu, and A. M. Minor, Nano Lett. **11**, 3207 (2011).

[18] B. Hu, Y. Zhang, W. Chen, C. Xu, and Z. L. Wang, Adv. Mater. **23**, 3536 (2011).

[19] P. Jin, G. Xu, M. Tazawa, and K. Yoshimura, Jpn. J. Appl. Phys. **41**, L278 (2002).

[20] X. Wu and G. C. Weatherly, Acta Mater. **47**, 3383 (1999).

[21] T. Tsuchiya, T. Taniwatari, M. Komori, R. Tsuneta, and H. Kakibayashi, Jpn. J. Appl. Phys. **33**, 230 (1994).

[22] M. D. Thouless, E. Olsson, and A. Gupta, Acta Metall. Mater. **40**, 1287 (1992).

[23] K. Okimura and J. Sakai, Jpn. J. Appl. Phys. **48**, 045504 (2009).

[24] T. Kanki, H. Takami, S. Ueda, A. N. Hattori, K. Hattori, H. Daimon, K. Kobayashi, and H. Tanaka, Phys. Rev. B **84**, 085107 (2011).

[25] P. Jin, S. Nakao, S. Tanemura, T. Bell, L. S. Wielunski, and M. V. Swain, Thin Solid Films **343-344**, 134 (1999).